

# Preparation and Electrochemical Properties of Porous Carbon Materials Derived from Waste Plastic Foam and Their Application for Supercapacitors

He Zhu, Songhong Fan, Zhishang Gao, Zhangzhang Tang, Zhong Ren, Mingjian Zhang, Huixia Feng, Heming Luo\*, Jianqiang Zhang\*

School of Petrochemical Engineering, Lan Zhou University of Technology, Lanzhou 730050, China

\*E-mail: [luohm666@163.com](mailto:luohm666@163.com), [zhangjq@lut.edu.cn](mailto:zhangjq@lut.edu.cn)

Received: 29 November 2020 / Accepted: 12 January 2021 / Published: 31 January 2021

---

In order to achieve resource recycling and environmental protection, the waste plastic foam-based porous carbon material PMC-T is prepared by a high-temperature pyrolysis activation method. Plastic foam-based porous carbon PMC-T is an amorphous carbon with a honeycomb-like structure, a specific surface area of up to 2281 m<sup>2</sup> g<sup>-1</sup>, and a reasonable pore size distribution. Cyclic voltammetry tests and galvanostatic charge/discharge tests show that the plastic foam-based porous carbon material PMC-700 exhibits excellent electrochemical performance. Specifically, in a 6 M KOH electrolyte at a 1 A g<sup>-1</sup> current density, the specific capacitance reached 296 F g<sup>-1</sup>. Additionally, PMC-T demonstrates good cycle stability, and after 5000 charging and discharging cycles, its capacitance retention rate is as high as 87.1%. The plastic foam-based porous carbon exhibits excellent electrochemical properties.

---

**Keywords:** Waste plastic foam; Porous carbon material; Supercapacitor; Specific surface area; Electrochemical performance

## 1. INTRODUCTION

As a main waste plastics pollution source, the plastic foam are commonly used and discarded directly. In order to achieve resource recycling and environmental protection, we focus on the preparation of porous carbon from waste plastic foam and its application in electrochemical energy storage. In the research of supercapacitors, electrode materials of supercapacitors have been paid much attention [1-8], the electrode materials used in supercapacitors should be such that the supercapacitor has a high specific capacitance and a long cycle life [9-12]. Electrical double-layer capacitor is a kind of supercapacitor. Electrical double-layer capacitor stores energy by forming a double-layer capacitance between electrode and electrolyte. The performance of electrical double-layer capacitor largely depend on the electrode material that contacts electrolyte ions, so the electrode material usually has rich holes

and high specific surface area [13-18]. Because porous carbon materials have the required characteristics of electrode material, we use porous carbon as electrode materials. Therefore, seeking a more effective preparation method to adjust the specific surface area and pore size distribution of the material is very important in the study of carbon materials. Zhang used waste polystyrene foam as a carbon source and silica particles to create a rich porous structure. The Friedel-Crafts reaction successfully produced a 3D network structure porous carbon material. The prepared material demonstrated a specific surface area of  $620 \text{ m}^2 \text{ g}^{-1}$  and a uniform mesopore distribution in the bulk phase. At a current density of  $1 \text{ A g}^{-1}$ , the specific capacitance of the prepared porous carbon material was  $208 \text{ F g}^{-1}$  [19]. Jiang used  $\text{CaCO}_3$  as a template and successfully converted polytetrafluoroethylene waste to porous carbon through the template carbonization method. When the mass ratio of PTFE: $\text{CaCO}_3$ : $\text{CO}(\text{NH}_2)_2$  was 2:1:2, the specific surface area was  $1048.2 \text{ m}^2 \text{ g}^{-1}$ , and when the current density was  $1 \text{ A g}^{-1}$ , the specific capacitance of the PTFE composite was  $237.8 \text{ F g}^{-1}$ . The results show that carbonization temperature and raw material mass ratio play a crucial role in regulating the pore structure [20].

Plastic foam is a kind of high molecular foam material. Due to its advantages of low density, corrosion resistance, moisture resistance, shock absorption, thermal insulation, and low cost, plastic is widely used and consumed in daily life. Additionally, waste plastic foam, often used as domestic waste, is discarded as high molecular waste that easily causes pollution to the environment. In this study, using waste PET plastic foam as the carbon source, argon as the protective gas, KOH as the activator, and a high-temperature pyrolysis chemical activation method, plastic foam-based porous carbon materials were prepared. The characterization and analysis of the microscopic morphology and structure, pore size distribution and surface functional groups of these materials were conducted. In a three-electrode system, in a 6 M KOH electrolyte, the effects of carbonization temperature and activator concentration on the electrochemical performance of the plastic foam-based porous carbon materials were investigated.

## 2. EXPERIMENTAL

### 2.1 Preparation of the plastic foam-based porous carbon material

#### 2.1.1 Preparation of carbonization

Discarded plastic foam was cut it into strips and placed into a porcelain boat; the boat was then placed into a tube furnace. Argon was used as a protective gas, and the furnace temperature was raised to  $600^\circ\text{C}$  at a rate of  $5^\circ\text{C}/\text{min}$ . The temperature was kept constant at  $600^\circ\text{C}$  for 2 h. After natural cooling, the product was collected, and the black carbonization powder was obtained by grinding.

#### 2.1.2 Preparation of the plastic foam-based porous carbon material

The obtained carbonization powder and KOH activator were evenly mixed and fully ground and then placed into a tube furnace under an atmosphere of argon gas as a protective gas. The sample was heated to a target temperature ( $600^\circ\text{C}$ ,  $700^\circ\text{C}$ ,  $800^\circ\text{C}$ ,  $900^\circ\text{C}$ ) at a rate of  $3^\circ\text{C}/\text{min}$  and was maintained

at a constant temperature for 2 h. After cooling to room temperature naturally, the black solid product was stirred and washed with 1 M hydrochloric acid solution. Then, the sample was repeatedly washed with ultrapure water until neutral, filtered and finally vacuum dried at 80°C for 12 h. A porous carbon material based on plastic foam was obtained. The porous carbon material was named PMC-T, wherein PM represents the plastic foam, C represents the carbon material, and T represents a target temperature.

In order to investigate the effect of the activator concentration on the capacitance performance of PMC-700 within PMC-700 and KOH with mass ratios of 1:2, 1:3, 1:4 and 1:5, were heated together at the carbonization temperatures of 700 ° C at a rate of 3°C/min and was maintained at a constant temperature for 2 h, followed by washing with 1 M HCl and deionized water until the pH of the filtrate was 7.0 and drying at 80 ° C for 12 h. the activation resulting products were denoted PMC-700-H(H-1:2,1:3,1:4 and 1:5)

## 2.2 Structure performance characterization

The crystal structure was characterized by X-ray diffraction (RINT-2000, Nippon Science), The test conditions are: radiation source is Cu K $\alpha$  ( $\lambda = 0.1541$ ), scanning range is 10 ~ 90 °, scanning speed is 15 ° min<sup>-1</sup>. The molecular vibration, rotation, and material properties of the carbon materials were characterized by Raman spectroscopy (JY-HR800, Horiba Scientific Group). The microstructure and morphology of the porous carbon materials were characterized by scanning electron microscopy (SEM, JSM-5600LV, JEOL) and transmission electron microscopy (TEM, JEM-1200EX, JEOL). The pore structure and pore size distribution of the carbon material were characterized by nitrogen adsorption/desorption tests (Tristar II 3020, Mike Instruments, USA). The N<sub>2</sub> adsorption amount under different relative pressures P/P<sub>0</sub> was measured at 77 K and liquid nitrogen temperature (-196 °C) and was determined by the BET method, where the specific surface, SBET, was calculated. The BJH method was used to fit the isotherm of the nitrogen adsorption/desorption and pore diameter distribution curve. X-ray photoelectron spectroscopy (ESCALAB 250Xi, Thermo Fisher Scientific) was used to identify the functional groups and elemental compositions on the surface of the carbon materials.

## 2.3 Electrochemical performance test

The working electrode was prepared by weighing 4 mg of the plastic foam-based porous carbon material and mixing it uniformly with acetylene black and polytetrafluoroethylene at a mass ratio of 8:1.5:0.5. Then, the material was made into a slurry with absolute ethanol, uniformly spread on a 1 cm × 1 cm nickel foam area, and vacuum dried at 80°C for 24 h. Then, the sample was kept at a pressure of 15 MPa for 1.5 min by a tableting machine to prepare an electrode sheet.

The electrochemical performance test was carried out in a three-electrode system consisting of the plastic foam-based porous carbon material as the working electrode, the 1.5 cm<sup>2</sup> platinum plate electrode as the opposite electrode, and the calomel electrode as the reference electrode. The electrolyte was a 6 M KOH solution. Cyclic voltammetry (CV) is a test method that characterizes the reaction on the electrode surface and discusses the mechanism of the electrode reaction. The parameters were set

between the voltage range of -1 V and 0 V and a scanning rate from 5 to 200 mV s<sup>-1</sup>. The specific capacitance  $C$  (F g<sup>-1</sup>) was calculated based on the following formula:

$$C = \frac{\int IdV}{2 \cdot v m \Delta V} \quad (1)$$

where  $I$  (A cm<sup>-2</sup>) is the current density,  $\Delta V$  (V) is the voltage window,  $m$  (g) represents the weight of active materials in the working electrode, and  $v$  (mV s<sup>-1</sup>) refers to the scanning rate.

The current charging and discharging test method investigates the potential change with time under a constant current, studies the performance of electrodes and capacitors, and calculates the specific capacitance. The galvanostatic charge/discharge (GCD) was tested under a voltage range of -1 V to 0 V and a charge-discharge current of 0.5 mA to 20 mA. The specific capacitance  $C$  (F g<sup>-1</sup>) is based on the following formula:

$$C = \frac{I \cdot \Delta t}{m \cdot \Delta V} \quad (2)$$

where  $I$  (A) is the charging and discharging current,  $\Delta V$  (V) is the voltage variation during the discharge time,  $\Delta t$ (s) is the discharge time, and  $m$  (g) is the mass of the porous carbon material on the working electrode.

Alternating current impedance (EIS) is a test method that disturbs capacitors with small AC amplitude signals and observes the system's reaction to disturbances from steady state. This method is also used to measure the AC impedance of electrodes and then calculates the electrochemical parameters of the electrodes. The AC impedance was measured in the frequency range of 0.01 Hz to 100 kHz, and the AC amplitude was 5 mV.

### 3. RESULTS AND DISCUSSION

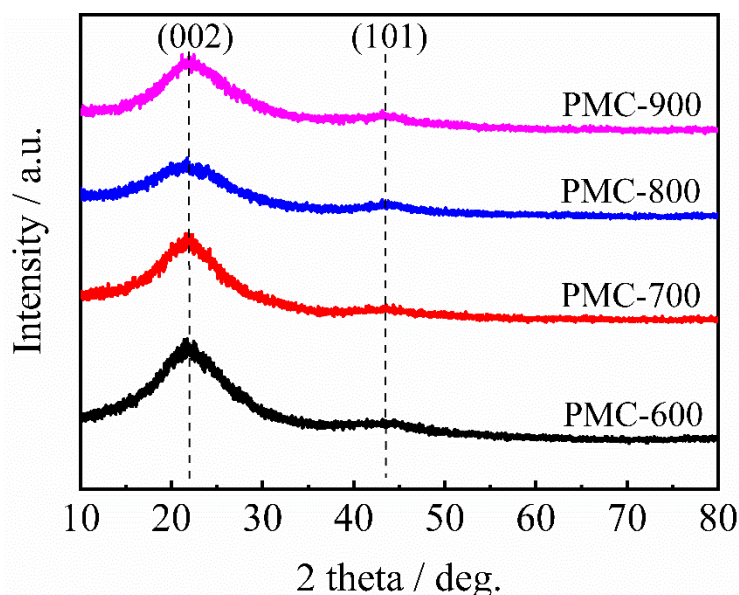


**Figure 1.** X-ray diffraction (XRD) spectra of PMC-T (target temperature are 600°C, 700°C, 800°C and 900°C)

Figure 1 shows the XRD spectra of the porous carbon material PMC-T. It can be seen from the figure that PMC-T exhibits two distinct diffraction peaks at diffraction angles of  $2\theta \approx 21.9^\circ$  and  $2\theta \approx 43.6^\circ$ , each corresponding to the (002) and (101) crystal planes of graphite, respectively. Compared with the standard graphite  $2\theta \approx 26.6^\circ$ , the (002) diffraction peak of PMC-T is located at  $21.9^\circ$ , and a significant shift occurs. According to the Bragg formula ( $2d \cdot \sin\theta = \lambda$ ), the interlayer distance of the (002) crystal plane of the porous carbon material PMC-T is increased [21,22]. The increase in the interlayer distance is mainly because during the chemical activation of high-temperature pyrolysis KOH, the generated K atom into the graphite layer of the graphite crystallite, resulting in an increase in the interlayer distance. It is known from this result that the porous carbon material PMC-T has an amorphous structure. The porous carbon material PMC-T has a low intensity (101) diffraction peak at a diffraction angle of  $43.6^\circ$ , indicating that this material contains flaky carbon nanostructures[23].

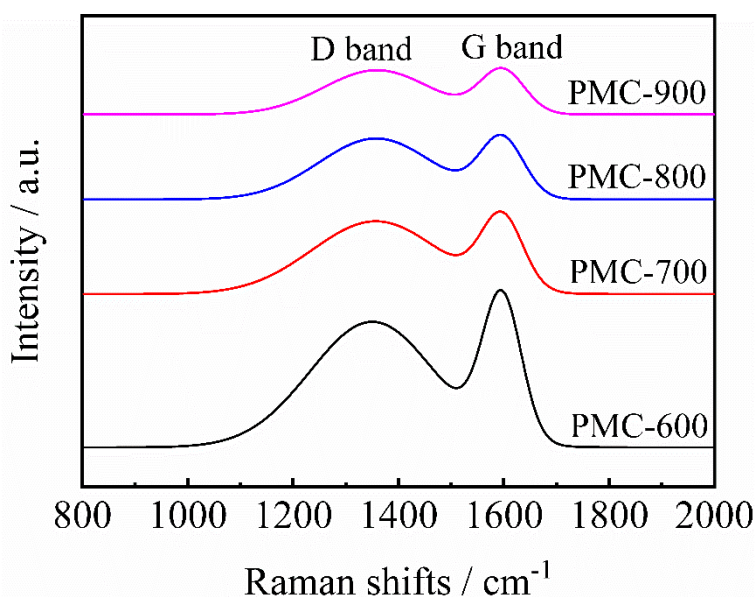


**Figure 2.** Raman spectroscopy of PMC-T (target temperature are 600°C, 700°C, 800°C and 900°C)

To further investigate the structure and degree of disorder of the porous carbon material PMC-T, the material was characterized by Raman spectroscopy. Figure 2 shows the Raman spectra of the porous carbon material PMC-T (600/700/800/900) at different carbonization temperatures. In the interval of 1000 ~ 1800, it can be seen that the Raman curve of the porous carbon material PMC-T has two typical peaks, corresponding to the D band at approximately  $1349 \text{ cm}^{-1}$  and the G band at approximately  $1593 \text{ cm}^{-1}$ . The D band reflects the disorder of the disordered carbon or the lattice structure, while the G band reflects the in-plane stretching vibration of the  $sp^2$  hybrid carbon atom  $E_{2g}$  phonon[24]. The  $I_D/I_G$  value is commonly used to calculate the intensity relationship of the two peaks. The larger the  $I_D/I_G$  value is, the higher the degree of the structural disorder of the carbon material is, and the lower the degree of graphitization is[25]. The  $I_D/I_G$  values of the porous carbon materials PMC-600, PMC-700, PMC-800, and PMC-900 are 1.523, 1.495, 1.447, and 1.339, respectively. As the carbonization temperature increases, the  $I_D/I_G$  value decreases accordingly. The results show that the

defects of the graphite layer of the carbon material gradually decrease and the degree of graphitization gradually increases.

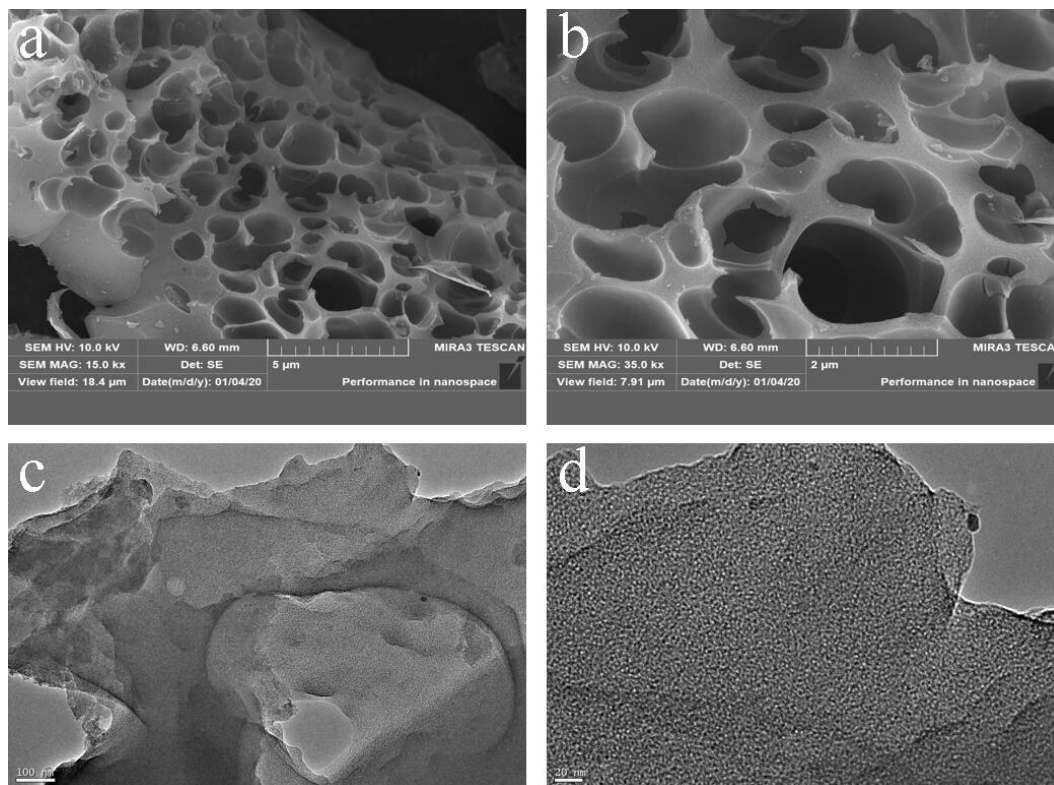


**Figure 3.** SEM (a, b) and TEM (c, d) images of PMC-700 (target temperature are 700°C)

To further observe and analyse the surface micromorphology and internal microchannel structure and size of PMC-T, SEM and TEM techniques were used. Figure 3(a, b) shows scanning electron micrographs of the porous carbon material PMC-700 at different magnifications, and the results indicate that PMC-700 has a honeycomb-like structure. This porous structure helps to increase the specific surface area, allows the electrolyte to immerse into the carbon material more smoothly, is beneficial for the rapid transfer of electrolyte ions, and effectively improves the electrochemical performance of the carbon material[26, 27]. Figure 3 (c, d) shows the transmission electron micrographs of PMC-700 at different high magnifications. Figure 3 (d) is a partially enlarged image of Figure 3 (c). It can be seen that the carbon material PMC-700 has a high degree of disorder, indicating that it has an amorphous structure, mainly due to the high-temperature pyrolysis activation process. The etching effect of KOH on the carbon material resulted in the increase of lattice defects, forming a rich and disordered pore structure.

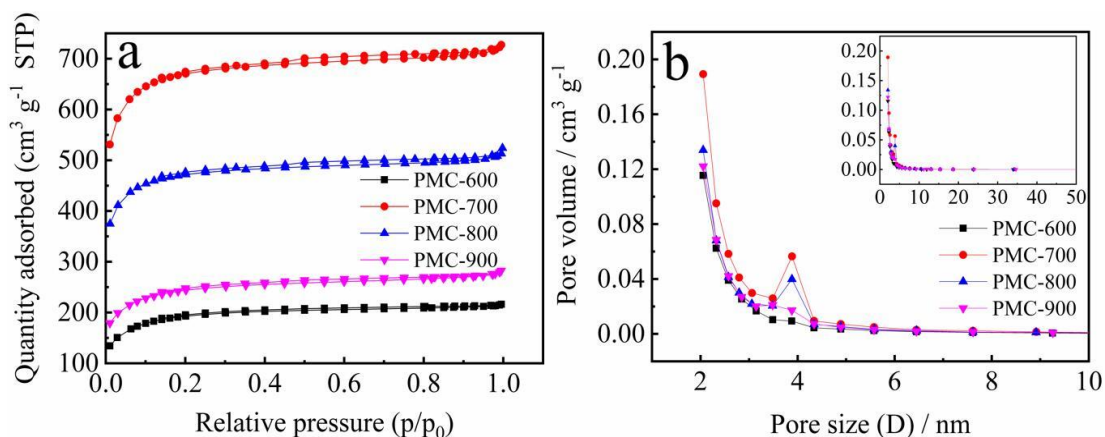


**Figure 4.** Nitrogen adsorption/desorption curve of PMC-T (target temperature are 600°C, 700°C, 800°C and 900°C) (a) and pore size distribution curve of PMC-T (target temperature are 600°C, 700°C, 800°C and 900°C) (b)

The nitrogen adsorption/desorption of the porous carbon material PMC-T is shown in Figure 4(a). The PMC-T curves can be classified as a I + IV type curve, which indicates that the porous carbon material PMC-T contains a large number of micro-mesoporous structures[28, 29]. When the relative pressure is below 0.01, the adsorption of N<sub>2</sub> is mainly performed by micropores, and the adsorption amount increases significantly, which means that the porous carbon material PMC-T has a rich micropore structure. When the relative pressure is close to 0.4, a more obvious H4 " hysteresis loop" appears, indicating that the material has a slit-like mesoporous structure. In the stage where the relative pressure (P/P<sub>0</sub>) rises from low to high pressure, the PMC-T curve shows a typical steady upward trend, which can be attributed to the increase in P/P<sub>0</sub>, which forces N<sub>2</sub> to enter the interior of the porous carbon caused by monolayer-multilayer N<sub>2</sub> adsorption. When the relative pressure is close to 1.0, the increase in N<sub>2</sub> adsorption of PMC-600, PMC-700, PMC-800, and PMC-900 is small, which shows that there are a few macroporous structures in PMC-600, PMC-700, PMC-800 and PMC-900. Figure 4 (b) shows the pore size distribution diagram of PMC-T. The material contains a large number of micro-mesopores, mainly concentrated near 2 nm, which is primarily caused by KOH activation during the high-temperature pyrolysis chemical activation process. At the same time, the porous carbon PMC-T also has an obvious peak at about 3.8 nm, indicating that the mesoporous distribution of the carbon material PMC-T is mainly concentrated in this range. As shown in Table 1, the average pore diameters of the porous carbon materials PMC-600, PMC-700, PMC-800, and PMC-900 are 1.97 nm, 1.94 nm, 1.95 nm, and 2.02 nm, respectively. Because the ion radius in the electrolyte is less than 0.4 nm, this type of aperture allows electrolyte ions to obtain a high-efficiency transmission channel and is beneficial for the generation of the electrical double-layer capacitance[30]. The specific surface areas of porous carbon materials PMC-600, PMC-700, PMC-800, and PMC-900 are 671 m<sup>2</sup> g<sup>-1</sup>, 2281 m<sup>2</sup> g<sup>-1</sup>, 1603 m<sup>2</sup> g<sup>-1</sup> and 842 m<sup>2</sup> g<sup>-1</sup>, respectively, and the specific surface area of PMC-T shows a trend of first increasing and then decreasing. This trend is mainly because high temperature plays a positive role in the activation of KOH during the pyrolysis activation process, which helps to increase the specific surface area. This

increase will cause the internal pores of the carbon material to collapse, resulting in a decrease in the specific surface area.

**Table 1.** Summary of the BET information for PMC-T (target temperature are 600°C, 700°C, 800°C and 900°C)

Samples	S <sub>BET</sub> (m <sup>2</sup> g <sup>-1</sup> )	Total Pore Volume (cm <sup>3</sup> g <sup>-1</sup> )	Average Pore Sizes (nm)
PMC-600	671	0.33	1.97
PMC-700	2281	1.11	1.94
PMC-800	1603	0.78	1.95
PMC-900	842	0.43	2.02

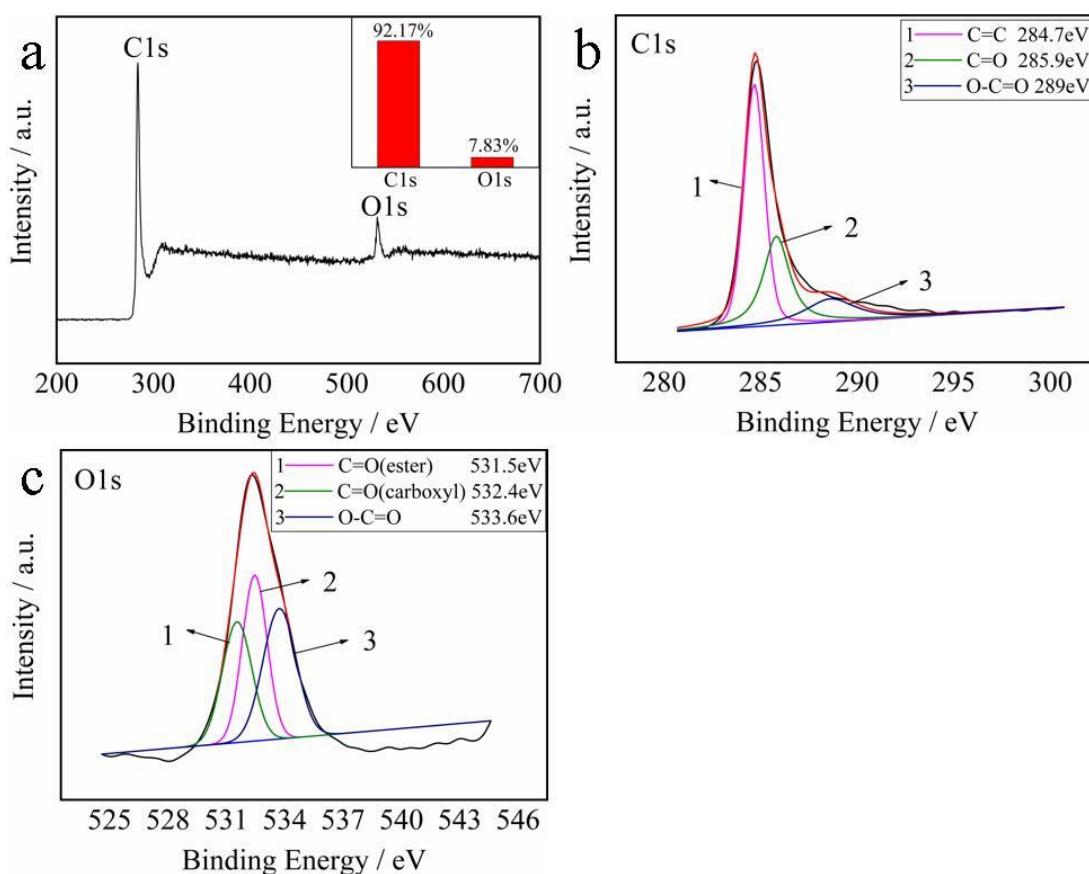


**Figure 5.** Elemental composition XPS spectrum for PMC-700 (target temperature are 700°C): full spectrum (a), C1s (b), and O1s (c)

X-ray photoelectron spectroscopy (XPS) was used to characterize the surface elements, content and surface functional groups of the porous carbon material PMC-700. The full XPS spectrum of PMC-

700 is shown in Figure 5(a). Two distinct peaks can be seen, corresponding to C1s and O1s, respectively. The contents of C and O accounted for 92.17% and 7.83%, respectively. Oxygen-containing functional groups can participate in the redox reactions to form pseudocapacitors, and these functional groups can also improve the wettability of the porous carbon materials[31, 32]. The C1s spectrum of PMC-700 is shown in Figure 5(b), and three peaks can be fitted: the peak with the highest intensity is located at 284.7 eV, corresponding to C=C; followed by the peak at 285.9 eV, corresponding to C=O; and the last characteristic peak at 289 eV corresponds to O-C=O[33-35]. Figure 5(c) is the O1s spectrum of PMC-700, which can fit three characteristic peaks, namely, the peak at 531.5 eV, which corresponds to C=O (ester) and the peaks at 532.4 eV and 533.6 eV, which correspond to C=O (carboxyl) and O-C=O, respectively[36, 37].

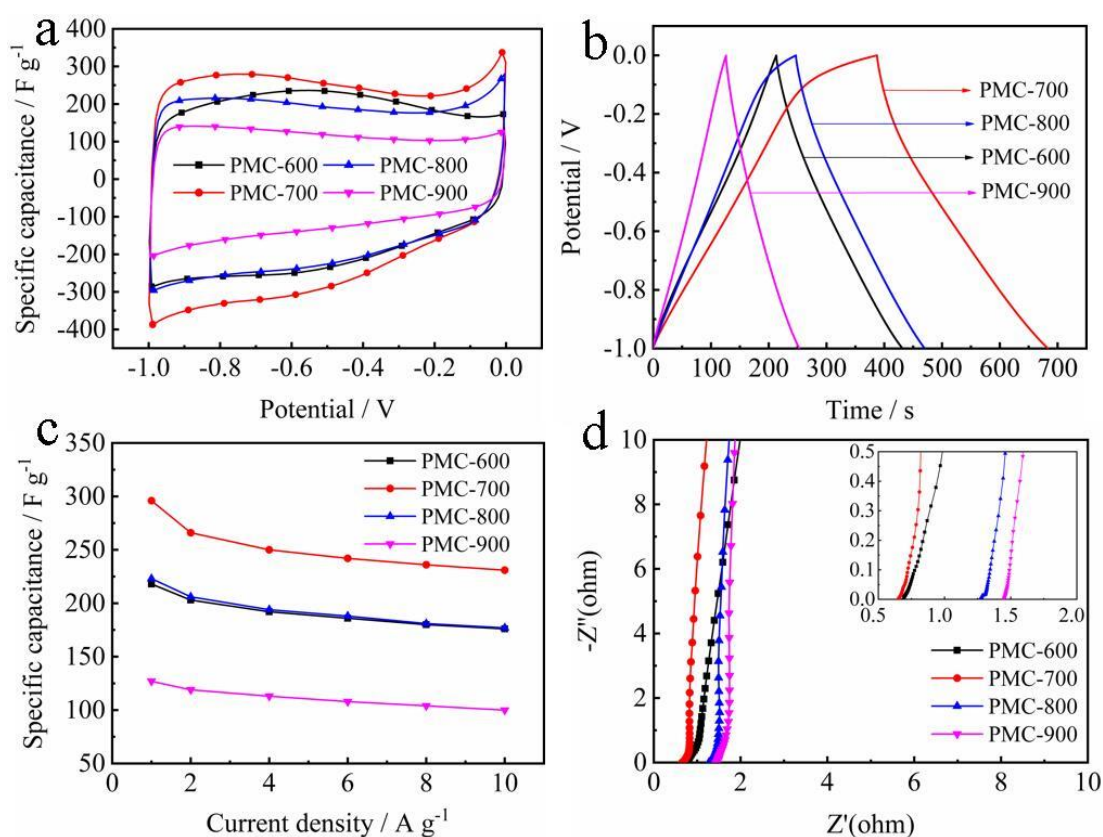


**Figure 6.** Electrochemical performance tests for PMC-T (target temperature are 600°C, 700°C, 800°C and 900°C): CV curve with a scanning rate of 10 mV s<sup>-1</sup> (a); GCD curve with a current density of 1 A g<sup>-1</sup> (b); specific capacitance based on the GCD curve (c); Nyquist plot (d)

Figure 6 (a) is the CV curve of the porous carbon material PMC-T obtained at different carbonization temperatures in a 6 M KOH electrolyte at a scanning rate of 10 mV s<sup>-1</sup>. Figure 6 (a) shows that there is a certain redox bump in the CV curve of PMC-T, which is mainly because the oxygen-containing surface functional groups present in the material participate in the redox reaction to produce a pseudocapacitance[38]. The CV curve of PMC-700 is calculated, and its graphic integral area is the largest, so it is known that PMC-700 has the best specific capacitance. Figure 6 (b) shows the GCD curve

of the porous carbon material PMC-T in the 6M KOH electrolyte at a current density of  $1 \text{ A g}^{-1}$ . From the figure, the GCD curves of PMC-700 and PMC-800 show a symmetrical triangular shape, and the curve deviating from the linear relationship once again illustrates the pseudocapacitance. According to the GCD curve calculation, at a current density of  $1 \text{ A g}^{-1}$ , the specific capacitance of PMC-600, PMC-700, PMC-800, and PMC-900 are  $218 \text{ F g}^{-1}$ ,  $296 \text{ F g}^{-1}$ ,  $223 \text{ F g}^{-1}$  and  $127 \text{ F g}^{-1}$ , respectively. The specific capacitance of PMC-700 is larger, which is the same as the result obtained by the CV curve of Figure 6 (a). Figure 6 (c) shows the specific capacitance at different current densities calculated at various temperatures according to the GCD curve. After a comparison, the capacitance performance of porous carbon PMC-700 is significantly better than that of the carbon materials at other temperatures. Because the material has a high specific surface area of  $2281 \text{ m}^2 \text{ g}^{-1}$  and a reasonable pore structure, the electrolyte can immerse into the carbon material more smoothly, which is beneficial for the rapid transfer of electrolyte ions and makes the specific surface area of the carbon material highly efficient. The utilization promotes an improvement in the electrochemical performance of the material. As the current density increases from  $1 \text{ A g}^{-1}$  to  $10 \text{ A g}^{-1}$ , the specific capacitance of PMC-700 decays from  $296 \text{ F g}^{-1}$  to  $231 \text{ F g}^{-1}$ , and its specific capacitance attenuation rate is approximately 22%, indicating that the porous carbon material PMC-700 has good rate performance.

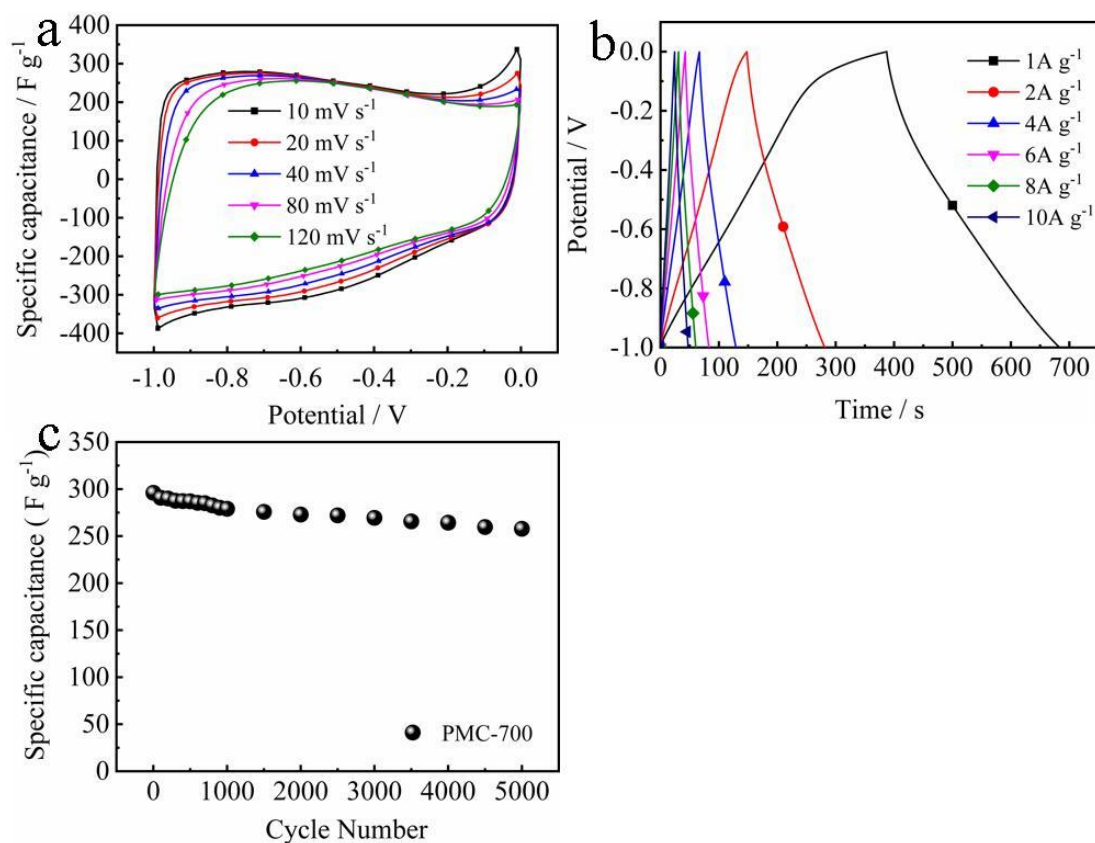


**Figure 7.** Electrochemical performance tests of PMC-700: CV curve at different scanning rates (a) (the different symbol segments show scanning rate); GCD curve at different current densities (b) (the different symbol segments show current densities); and cycle life test (c) (current density  $1 \text{ A g}^{-1}$ )

The Nyquist diagram of PMC-T is shown in Figure 6 (d). In the low frequency region, the curves of the porous carbon materials PMC-600, PMC-700, PMC-800, and PMC-900 are nearly perpendicular to the horizontal axis. This finding means that the material PMC-T has excellent capacitor performance. At the same time, in the high frequency region, the alternating current series resistance (ESR) of the porous carbon materials PMC-600, PMC-700, PMC-800, and PMC-900 are 0.69  $\Omega$ , 0.65  $\Omega$ , 1.27  $\Omega$ , and 1.45  $\Omega$ , respectively. It can be observed that there is a less obvious semi-circle structure in the high frequency region, indicating that the porous carbon material PMC-T has a very small pseudo charge-transfer resistance and can perform faster charge transfer[39].

In Figure 7(a), the CV curves of the porous carbon material PMC-700 at different scanning rates are shown, and it can be observed that PMC-700 maintains good capacitance performance at different scanning rates. Figure 7(b) shows the GCD curve of PMC-700 at different current densities; it is easy to see that the GCD curve does not demonstrate a good linear relationship, proving that this material exhibits both double capacitance and pseudocapacitance performance, and with increasing current density, the GCD curve profile of the material approaches an isosceles triangle. This result is largely due to the shortening of the charging and discharging time at high current density, which means the electrolyte ions do not have enough time to enter the internal pores of the carbon material, and the contribution of the pseudocapacitance to the capacitance is reduced; therefore, the GCD curve profile approaches an isosceles triangle[40]. Figure 7(c) is a cycle life test. At a current density of 1 A g<sup>-1</sup>, after 5000 cycles of galvanostatic charge/discharge, the capacity retention rate of the porous carbon material PMC-700 is 87.1%, and the material shows good stability.

According to the characterization and test results of the porous carbon material PMC-T, it can be found that the porous carbon material PMC-T prepared by high-temperature pyrolysis activation method has excellent electrochemical performance. As shown in Table 2, PMC-700 is compared with similar electrode materials for supercapacitors described in literature, and it is found that it has a good performance in terms of specific surface, specific capacitance and cycle life.

**Table 2.** Comparison of the material with similar electrode materials for supercapacitors described in literature

sample	specific capacitance (F g <sup>-1</sup> )	capacity retention rate (after 5000 cycles)	specific surface (m <sup>2</sup> g <sup>-1</sup> )	Refs
PC	208 (current density 1 A g <sup>-1</sup> )	94.3% (after 5,000 cycles at 5 A g <sup>-1</sup> )	620	[22]
carbon-2:1:2	237.8 (current density 1 A g <sup>-1</sup> )	97.60% (after 10,000 cycles at 10 A g <sup>-1</sup> )	1048.2	[23]
PMC-700	296 (current density 1 A g <sup>-1</sup> )	87.1% (after 5,000 cycles at 1 A g <sup>-1</sup> )	2281	This work

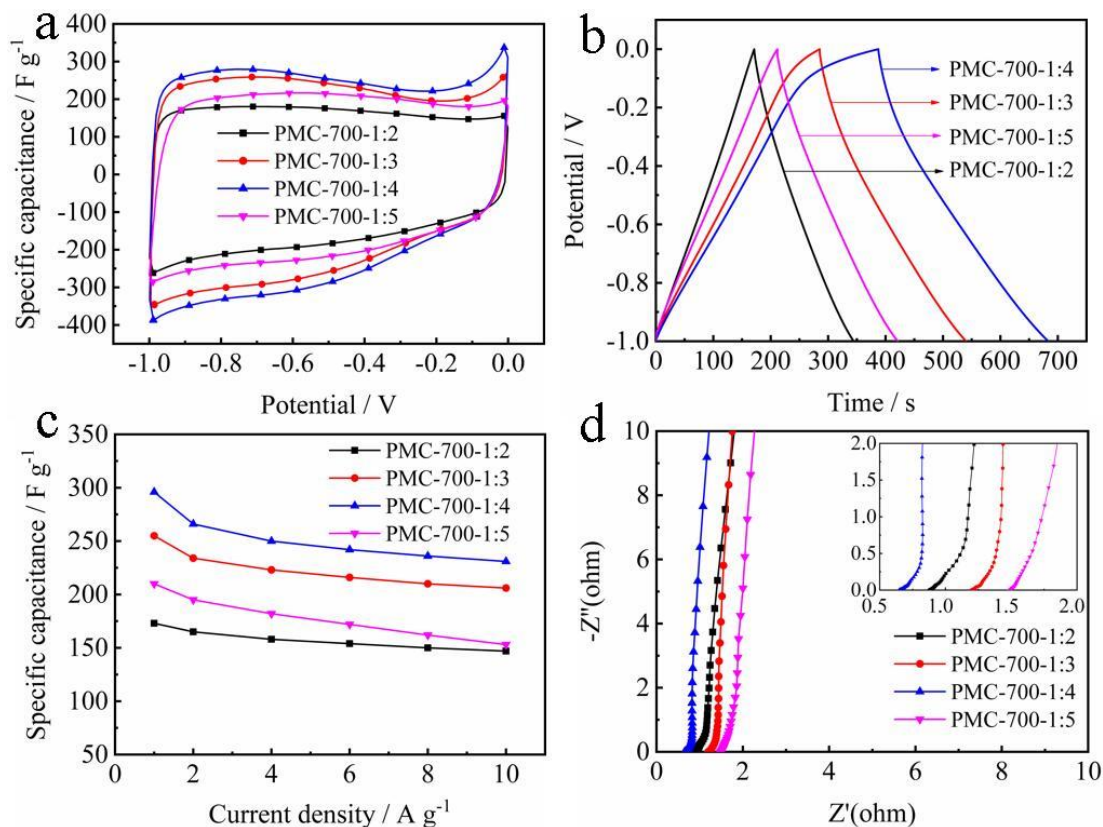


**Figure 8.** Electrochemical performance tests of PMC-700-H (H-1:2,1:3,1:4,1:5): CV curve with a scanning rate of  $10 \text{ mV s}^{-1}$  (a); GCD curve with a current density of  $1 \text{ A g}^{-1}$  (b); specific capacitance based on the GCD curve (c); Nyquist plot (d)

The effect of the activator concentration on the capacitance performance of PMC-700 during the activation process was further investigated. Figure 8 (a) shows the foam-based porous carbon PMC-700-H prepared with different carbon-alkali ratios in a 6 M KOH electrolyte. The CV curve measurements were performed at a scanning rate of  $10 \text{ mV s}^{-1}$ . As seen from Figure 8 (a), there is a certain redox bump in the CV curve of the porous carbon material PMC-T, which is caused by the oxygen functional groups in the material. The CV curve of PMC-700-1:4 is calculated, and its graphic integral area is the largest, so it is known that PMC-700-1:4 has the largest specific capacitance. Figure 8 (b) shows the GCD curve of the porous carbon material PMC-700-H in a 6 M KOH electrolyte at a current density of  $1 \text{ A g}^{-1}$ . It can be seen from the figure that the PMC-700-1:3 and PMC-700-1:4 show a more obvious asymmetrical triangular, which also demonstrates pseudocapacitance performance. According to the GCD curve calculation, at a current density of  $1 \text{ A g}^{-1}$ , the specific capacitances of PMC-700-1:2, PMC-700-1:3, PMC-700-1:4, and PMC-700-1:5 are  $173 \text{ F g}^{-1}$ ,  $255 \text{ F g}^{-1}$ ,  $296 \text{ F g}^{-1}$  and  $210 \text{ F g}^{-1}$ , respectively. Figure 8(c) shows the change trend of the specific capacitance of the porous carbon material PMC-700-H calculated according to the GCD curve at different current densities. After a comparison, for the porous carbon material PMC-700-1:4, the specific capacitance is the largest, and the rate performance is good. The Nyquist diagram of PMC-700-H is shown in Figure 8 (d). In the low frequency region, the curves

of PMC-700-1:2, PMC-700-1:3, PMC-700-1:4, and PMC-1:5 and the horizontal axis show a good vertical relationship, indicating that the PMC -700-H exhibits excellent capacitance performance. At the same time, in the high frequency region, the alternating current series resistance (ESR) is 0.88  $\Omega$ , 1.20  $\Omega$ , 0.65  $\Omega$ , and 1.49  $\Omega$ . It can be seen that the porous carbon material PMC-700-1:4 has the smallest AC series resistance, and all samples in the high frequency area do not contain obvious semi-circle. The semi-circle indicates that the material has a very small pseudocharge transfer resistance, which enables faster charge transfer[39].

#### 4. CONCLUSION

In this paper, using waste plastic foam as the carbon source, the plastic foam-based porous carbon material PMC-T is prepared by pre-carbonization-KOH activation. With the help of a series of characterization methods, it is known that the porous carbon material PMC-T is amorphous carbon. The porous carbon material PMC-700 has a specific surface area of up to 2281  $\text{m}^2 \text{g}^{-1}$ . The porous carbon PMC-T mainly exhibits a micro-mesoporous structure, which contributes to the efficient transport of electrolyte ions and an improvement in the electrochemical performance. The material exhibits excellent electrochemical performance. In a 6 M KOH electrolyte with a current density of 1  $\text{A g}^{-1}$ , the specific capacitance of PMC-700 is as high as 296  $\text{F g}^{-1}$ . Additionally, the material demonstrates good rate performance. As the current density increases from 1  $\text{A g}^{-1}$  to 10  $\text{A g}^{-1}$ , the specific capacitance decreases from 296  $\text{F g}^{-1}$  to 231  $\text{F g}^{-1}$ , and the attenuation rate is only 22%. After 5000 cycles of galvanostatic charge/discharge, the specific capacitance retention rate of PMC-700 was 87.1%, showing excellent stability. We believe that the application of solid waste polymer materials in the preparation of a promising electrode material for supercapacitors application. has certain potential value and helps alleviate the white pollution problem.

#### DECLARATION OF INTERESTS

On behalf of all authors, the corresponding author states that there is no conflict of interest.

#### ACKNOWLEDGEMENTS

This effort was supported by the National Natural Science Foundation of China (21364004 and 21664009), Gansu Province University Fundamental Research Funds and Doctor Research Fund of Lanzhou University of Technology, P.R. China.

#### References

1. S. A. Haladkar, M. A. Desai, S. D. Sartale and P. S. Alegaonkar, *J. Mater. Chem. A*, 6 (2018) 7246.
2. D. Hu, C. Y. Chen and Q. Liu, *J. Mater. Sci.*, 53 (2018) 12310.
3. J. Y. Piao, D. S. Bin, S. Y. Duan, X. J. Lin, D. Zhang and A. M. Cao, *Sci. China Chem.*, 61 (2018) 538.

4. W. J. Lu, M. X. Liu, L. Miao, D. Z. Zhu, X. Wang, H. Duan, Z. W. Wang, L. C. Li, Z. J. Xu, L. H. Gan and L. W. Chen, *Electrochim. Acta*, 205 (2016) 132.
5. M. Yu, Y. X. Ma, J. H. Liu and S. M. Li, *Carbon*, 87 (2015) 98.
6. K. V. Sankar, Y. Seo, S. C. Lee and S. C. Jun, *ACS Appl. Mater. Interfaces*, 10 (2018) 8045.
7. C. Kim, B. T. Ngoc, K. S. Yang, M. Kojima, Y. A. Kim, Y. J. Kim, M. Endo and S. C. Yang, *Adv. Mater.*, 19 (2007) 2341.
8. W. Du, Y. L. Bai, J. Q. Xu, H. B. Zhao, L. Zhang, X. F. Li and J. J. Zhang, *J. Power Sources*, 402 (2018) 281.
9. Y. Zhang, H. Feng, X. Wu, L. Wang, A. Zhang, T. Xia, H. Dong, X. Li and L. Zhang, *Int. J. Hydrogen Energy*, 34 (2009) 4889.
10. M. M. A, C. A. B and F. S. A, *Solid State Ionics*, 148 (2002) 493.
11. Y. Gong, D. Li, C. Luo, Q. Fu and C. Pan, *Green Chem.*, 19 (2017) 4132.
12. J. Jiang, Y. Zhang, P. Nie, G. Xu and X. Zhang, *Adv. Sustainable Syst.*, 2 (2017) 1700110.
13. Q. F. Meng, K. F. Cai, Y. X. Chen and L. D. Chen, *Nano Energy*, 36 (2017) 268.
14. X. J. He, X. J. Li, H. Ma, J. F. Han, H. Zhang, C. Yu, N. Xiao and J. S. Qiu, *J. Power Sources*, 340 (2017) 183.
15. S. Joseph, D. M. Kempaiah, M. R. Benzigar, H. Ilbeyg, G. Singh, S. N. Talapaneni, D. H. Park and A. Vinu, *Microporous Mesoporous Mater.*, 280 (2019) 337.
16. C. Noh and Y. Jung, *Phys. Chem. Chem. Phys.*, 21 (2019) 6790.
17. E. Lim, C. Jo and J. Lee, *Nanoscale*, 8 (2016) 7827.
18. P. Sharma and T. S. Bhatti, *Energy Convers. Manage.*, 51 (2010) 2901.
19. Y. X. Zhang, Z. M. Shen, Y. F. Yu, L. Liu, G. X. Wang and A. B. Chen, *J. Mater. Sci.*, 53 (2018) 12115.
20. W. M. Jiang, X. H. Jia, Z. J. Luo and X. Y. Wu, *Electrochim. Acta*, 147 (2014) 183.
21. Y. Wang, F. B. Su, C. D. Wood, J. Y. Lee and X. S. Zhao, *Ind. Eng. Chem. Res.*, 47 (2008) 2294.
22. R. R. Rajagopal, L. S. Aravinda, R. Rajarao, B. R. Bhat and V. Sahajwalla, *Electrochim. Acta*, 211 (2016) 488.
23. H. M. Luo, Y. F. Yang, Y. Z. Chen, J. Q. Zhang and X. Zhao, *J. Appl. Electrochem.*, 46 (2016) 113.
24. R. Zeng, X. N. Tang, B. Y. Huang, K. Yuan and Y. W. Chen, *Chemelectrochem*, 5 (2018) 515.
25. Z. J. Tang, Z. X. Pei, Z. F. Wang, H. F. Li, J. Zeng, Z. H. Ruan, Y. Huang, M. S. Zhu, Q. Xue, J. Yu and C. Y. Zhi, *Carbon*, 130 (2018) 532.
26. M. E. Abdelsalam, I. Elghamry, A. H. Touny and M. M. Saleh, *J. Appl. Electrochem.*, 49 (2019) 45.
27. N. Manyala, A. Bello, F. Barzegar, A. A. Khaleed, D. Y. Momodu and J. K. Dangbegnon, *Mater. Chem. Phys.*, 182 (2016) 139.
28. Y. M. Lian, M. Ni, Z. H. Huang, R. J. Chen, L. Zhou, W. Utetiwabo and W. Yang, *Chem. Eng. J.*, 366 (2019) 313.
29. V. Gómez-Serrano, C. González-García and M. González-Martín, *Powder Technol.*, 116 (2001) 103.
30. Y. P. Zhai, Y. Q. Dou, D. Y. Zhao, P. F. Fulvio, R. T. Mayes and S. Dai, *Adv. Mater.*, 23 (2011) 4828.
31. J. J. Zhang, H. X. Fan, X. H. Dai and S. J. Yuan, *R. Soc. Open Sci.*, 5 (2018) 172456.
32. L. Luo, T. Chen, Z. Li, Z. Zhang, W. Zhao and M. Fan, *J. CO2 Util.*, 25 (2018) 89.
33. S. B. Kulkarni, U. M. Patil, I. Shackery, J. S. Sohn, S. Lee, B. Park and S. Jun, *J. Mater. Chem. A*, 2 (2014) 4989.
34. X. J. Liu, Y. C. Zhou, W. J. Zhou, L. G. Li, S. B. Huang and S. W. Chen, *Nanoscale*, 7 (2015) 6136.
35. Q. Wang, J. Yan, Y. B. Wang, T. Wei, M. L. Zhang, X. Y. Jing and Z. J. Fan, *Carbon*, 67 (2014) 119.
36. M. A. Patel, F. X. Luo, K. Savaram, P. Kucheryavy, Q. Q. Xie, C. Flach, R. Mendelsohn, E. Garfunkel, J. V. Lockard and H. X. He, *Carbon*, 114 (2017) 383.
37. Y. Y. Wen, B. Wang, C. C. Huang, L. Z. Wang and D. Hulicova-Jurcakova, *Chem. - Eur. J.*, 21

(2015) 80.

38. J. Q. Zhang, S. Y. Song, J. C. Xue, P. Li, Z. S. Gao, Y. B. Li, Z. Zhang, H. X. Feng and H. M. Luo, *Int. J. Electrochem. Sci.*, 13 (2018) 5204.
39. C. S. Yang, Y. S. Jang and H. K. Jeong, *Curr. Appl Phys.*, 14 (2014) 1616.
40. B. Y. Guan, A. Kushima, L. Yu, S. Li, J. Li and X. W. Lou, *Adv. Mater.*, 29 (2017).

© 2021 The Authors. Published by ESG ([www.electrochemsci.org](http://www.electrochemsci.org)). This article is an open access article distributed under the terms and conditions of the Creative Commons Attribution license (<http://creativecommons.org/licenses/by/4.0/>).